RASĀYAN *J. Chem.*
Vol. 16 | No. 4 |2109-2118| October - December | 2023
ISSN: 0974-1496 | e-ISSN: 0976-0083 | CODEN: RJCABP
http://www.rasayanjournal.com
http://www.rasayanjournal.co.in

INTENSE RED-LIGHT EMITTING Eu^{+3} IONS IN B_2O_3-ZnF_2-CaF_2-Al_2O_3 GLASSES FOR LASER APPLICATIONS

N. Rajya Lakshmi[1,2], Santhan Kumar Jalli[1], K. Venkatarao[1,3] and Sandhya Cole[1,✉]

[1]Department of Physics, Acharya Nagarjuna University, Nagarjuna Nagar, Guntur-522510, India
[2]Department of Physics, Govt. Polytechnic College, Repalle-522265, Andhra Pradesh, India
[3]Department of Physics, Government Institute of Textile Technology, Guntur-522005, Andhra Pradesh, India
Corresponding Autor: sandhya.cole@gmail.com

ABSTRACT

The current study examines the effect of Eu^{3+} ions on B_2O_3-ZnF_2-CaF_2-Al_2O_3 glasses. These are examined by XRD, FT-IR, absorption, excitation, and emissions studies. From these studies, XRD, FT-IR, absorption, excitation, and emissions are also calculated and it reveals the presence of a covalent nature exists in glass materials. From these emission spectra, J-O parameters, transition probabilities (A_τ), radioactive lifetime (τ_R), and branching ratio (β_r) color (CIE) coordinates are estimated. All the above studies indicate that these materials are appropriate for red-light laser source applications.

Keywords: XRD: FT-IR: Optical Absorption: Naphelauxetic ratio: Emission Spectra: J-O parameters.
RASĀYAN*J. Chem.*, Vol. 16, No. 4, 2023

INTRODUCTION

Nowadays, more emphasis is placed on the spectroscopic features of RE^{3+} ions doped glasses for the expansion of optical materials such as optical detectors, display devices, energy converters, optical amplifiers, and so on. Because of the simplicity of the energy level structure with non-degenerate ground state $^7F_0$ to the excited of $^5D_0$.[1] Eu^{3+} doped glasses were chosen for red emission among several rare earth-doped materials. Because of the strong emission band in UV-Vis regions and the availability of appropriate activators for red-light emission, the hypersensitivity and electric dipole transition of $^5D_0 \rightarrow {}^7F_2$ about 612 nm of Eu^{3+} ions doped red phosphors are often employed in the field of emission technology. Based on the host glass matrix, these Eu^{3+} ions play a vital function in commercial and technical applications.[2] In addition to rare-earth ions, oxide glasses are shown to be chemically stable and the best choice due to their transparency, good rare-earth compatibility, high phonon energy, poor quantum efficiency, and enhancement of luminescence features. Borate (B_2O_3) glasses are generally fascinating materials because of their high transparency, high thermal stability, strong chemical and mechanical strength, and rare earth compatibility due to structural and physical properties.[3] The borate glass system has trigonal (BO_3) and tetrahedral (BO_4) units of B_2O_3. However, these glasses have high phonon energy, which causes non-radiative transitions and results in low phonon and quantum efficiency. The addition of a modifier such as ZnF_2 into the borate glass matrix, where fluorine ions replace oxide ions, is predicted to increase the range of glass formation and glass stability.[4] Because of these ZnF_2, the viscosity of the glasses is reduced, the transparency is improved, and the glasses are more resistant to moisture. Together with ZnF_2, another fluoride, such as CaF_2, is employed to change the structure of the glass inside the glass network, as well as to increase the physical and chemical endurance of the materials.[5] Incorporation of Al_2O_3 into the glass system makes the glass more resistant. Because of the strong mechanical and chemical strength, and chemical durability of Al^{3+} ions at the borate system with the high glass transition temperature, The Al^{3+} ions engaged based on a network with various structural units of AlO_4 and AlO_6 improving the mechanical and electrical characteristics of glass materials.[6] Taking into account the aforesaid scientific benefits provided by chemicals such as H_3BO_3, ZnF_2, CaF_2, Al_2O_3,

http://doi.org/10.31788/RJC.2023.1648425

and Eu_2O_3, a novel optical system, namely B_2O_3-ZnF_2-CaF_2-Al_2O_3 glasses, is developed, and these are defined by structural features depending on the varying concentrations of the Eu^{3+} ions.

EXPERIMENTAL

The examined glasses were created by combining analytical grade with 99.99% pure components such as H_3BO_3, ZnF_2, CaF_2, Al_2O_3, and Eu_2O_3. The chemical composition of the examined glasses (in mol%) is 55 B_2O_3-(25-x) ZnF_2-10CaF_2-10Al_2O_3-xEu_2O_3 (where x=0.1, 0.3, 0.5, 0.7, and 0.9). Each system's glass batches were weighted and carefully mixed in an agate motor before being pulverized into a fine powder. The combined powder samples are placed in silicon crucibles and melted at a temperature of 1200 degrees Celsius in an electric furnace. The molten metal was placed over a hot brass plate. To prevent thermal stress, the glass samples were annealed at 300°C for 4 hours before being cooled to ambient temperature. The annealed glass samples were polished and cut to the dimensions of 1x2x1 cm.

RESULTS AND DISCUSSION

Physical Properties

To determine the compactness of glass materials, fundamental physical characteristics like density, refractive index, RE ion concentration, polaron radius etc. are computed, as shown in Table-1. Because of structural alterations and geometrical configurations of the glass components, the density of the examined glasses rises somewhat as the concentration of Eu_2O_3 increases. Because of the high compactness of the structure of glass, the values of the refractive index and density rise. Since Eu_2O_3 functions as a network moderator, the compactness of glass materials diminishes as the concentration of Eu^{3+} ions increase.[7] Figure-1 depicts the density and refractive index variations of the B_2O_3-ZnF_2-CaF_2-Al_2O_3-Eu_2O_3 glasses. The reduction in polaron radius demonstrates that increasing the concentration of Eu^{3+} ions lead to an increase the compactness of glass network and the formation of a strong connection between Eu and the oxygen ligand.

XRD

The XRD pattern of the studied glasses reveals that no crystalline peaks, indicating the glass materials are amorphous seen in Fig.-2.

FT-IR Spectra

Infrared spectroscopy is used to characterize the structural characteristics and disorder of glass materials. Figure-3 depicts the FT-IR spectra acquired at room temperature in the range 400 to 1400 cm^{-1}. The B-O-B connection in the borate network is responsible for the band centered at 685 cm^{-1}. Another band is linked to the combined stretching vibrations of the structural components BO_4 and AlO_4 units respectively.

Table-1: Physical Parameters of Eu^{3+} Doped B_2O_3-ZnF_2-$CaF_2Al_2O_3$ Glasses

No.	Physical parameters	E_0	E_1	E_3	E_5	E_7	E_9
1	Density ρ (g/cm^3) (± 0.0001)	2.9162	2.9063	2.9106	2.9223	2.9316	2.9403
2	Average molecular weight M(g/mol)	82.144	82.393	82.890	83.387	83.884	84.381
3	Ion concentration N_i (10^{20} ions/cm^3) (± 0.001)	-	0.2141	0.6343	1.0552	1.4731	1.8820
4	Interionic distance r_i (Å) (± 0.001)	-	36.102	25.073	21.162	18.933	17.420
5	Polaron radius r_p (Å) (± 0.001)	-	14.548	10.102	8.526	7.628	7.022
6	Field strength F_i (10^{14} cm^{-2}) (± 0.001)	-	1.6051	3.1775	4.5914	5.8401	6.8368
7	Refractive index n_d (-) (± 0.0001)	1.6562	1.6598	1.6623	1.6645	1.6762	1.6863

8	Reflection loss R (-)	0.0322	0.0325	0.0327	0.0328	0.0338	0.0346
9	Molar reflectivity R_M (cm^{-3}) ($\pm$ 0.001)	8.8199	8.6825	9.3801	9.0240	8.9279	9.1678
10	Optical dielectric constant ε (-) ($\pm$ 0.001)	2.7429	2.7549	2.7632	2.7705	2.8096	2.8436

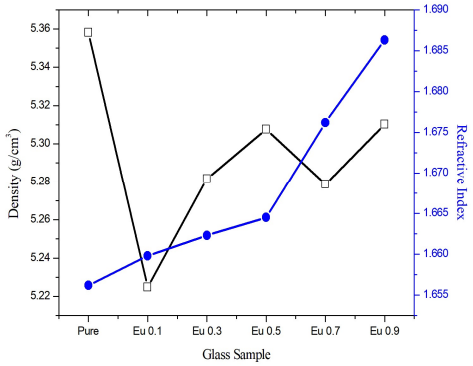

Fig.-1: The variation of the density and refractive index of Eu^{3+} doped B_2O_3-ZnF_2-CaF_2-Al_2O_3 glasses

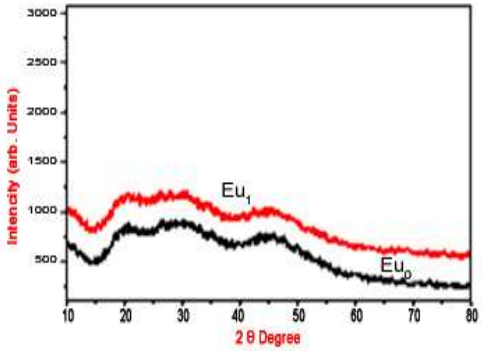

Fig.-2: XRD spectra of Eu^{3+} doped B_2O_3-ZnF_2-CaF_2-Al_2O_3 glasses

The band at 1055 cm^{-1} is attributed to symmetric vibrations of BO_3 and AlO_4 structural units.[8] The wide band of about 1226 cm^{-1} is caused by asymmetric vibrations of the Pyro, ortho borate group in the B-O bond, as shown in Table-2. Because of the low concentration, the influence of Eu^{3+} ions on the produced glasses has no effect, and the structural bonds remain unaltered.

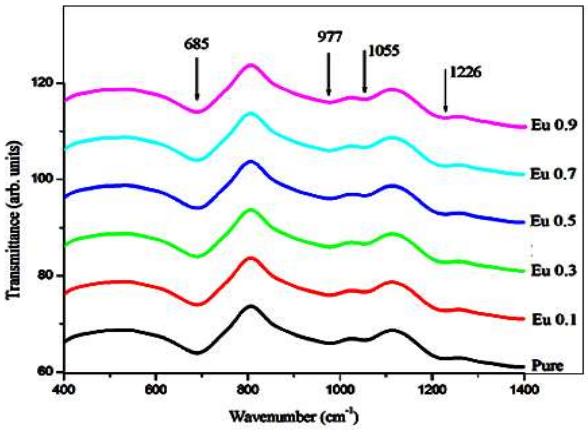

Fig.-3: FTIR spectra of Eu^{3+} doped B_2O_3-ZnF_2-CaF_2-Al_2O_3 glasses

Absorption Spectra

The absorption spectrum of Eu^{3+} doped B_2O_3-ZnF_2-CaF_2-Al_2O_3 glasses was taken at 28^0C temperature with a wavelength range of 350-2250 nm. All concentrations are recorded from these spectra and appear similar band intensities. The band intensity rises as the composition of Eu^{3+} ions increases. Figure-4(a)

depicts the distinctive absorption bands of UV-VIS spectra, whereas Fig.4-(b) depicts the NIR region spectra. Based on the f-f transitions from the $^7F_0$ ground state to the thermally excited $^7F_1$ level of Eu^{3+} ions, the observed bands are inhomogeneous.[9] The UV-Vis band corresponds to $^7F_0 \rightarrow {}^5L_6$, $^5D_2$, $^5D_1$, and $^7F_1 \rightarrow {}^5L_6$, $^5D_3$. The bands in the NIR region correspond to the transitions $^7F_0 \rightarrow {}^7F_6$ and $^7F_1 \rightarrow {}^7F_6$.

Table-2: FT-IR Band Positions of Eu^{3+} Doped B_2O_3-ZnF_2-$CaF_2Al_2O_3$ Glasses

Band Positions (cm^{-1})	Band Assignment
685	B-O-B linkage in the borate network
977	Combined stretching vibrations of BO_4 and AlO_4 structural units
1055	Symmetric vibrations of BO_3 and AlO_4 Structural Units
1226	B-O bond asymmetric stretching vibrations of pyro, ortho borate group

Table-3: The Evaluated Parameters of Direct, Indirect, and Urbach Values of Eu3 + doped B_2O_3-ZnF_2-CaF_2-Al_2O_3 Glasses

Glass Samples	Theoretical band gap	Direct band gap (eV)	Indirect band gap (eV)	Urbach energy (eV)
Eu 0.1	365	3.409	3.564	0.293
Eu 0.3	364	3.421	3.572	0.292
Eu 0.5	356	3.486	3.583	0.287
Eu 0.7	354	3.507	3.596	0.285
Eu 0.9	352	3.515	3.617	0.284

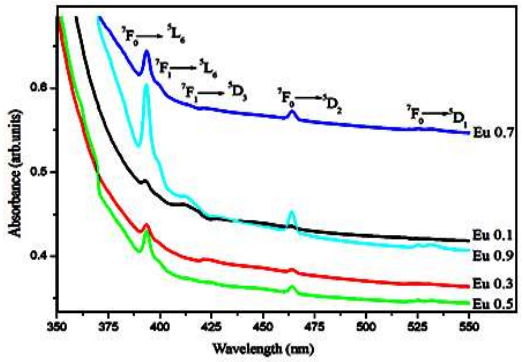

Fig.-4(a): Optical absorption spectrum of Eu^{3+} B_2O_3-ZnF_2-CaF_2-Al_2O_3 glasses in visible region

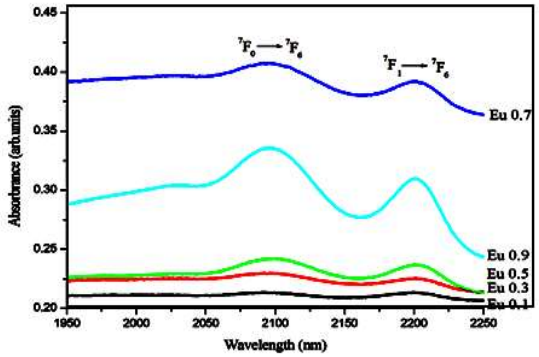

Fig.-4(b): Optical absorption spectrum doped of Eu^{3+} doped B_2O_3-ZnF_2-CaF_2-Al_2O_3 glasses in NIR region

Optical Energy Band Gap (E_{opt}) Urbach Energy (ΔE)

The optical band gap for the Eu^{3+} doped B_2O_3-ZnF_2-CaF_2-Al_2O_3 glasses may be determined to define the nature of the materials. The absorption coefficient (v) of the curve's edge is estimated using the formula

$$\alpha(\nu) = \frac{1}{d}\log\left(\frac{I_0}{I_t}\right) \qquad (1)$$

Here I_0 and I_t are the incident and transmitted intensities of the beam, and d is the sample thickness. The absorbance is represented by the coefficient factor log (I_o/I_t). The expression for band gap transitions can be estimated with photon energy hν as a point of the absorption coefficient.

$$\alpha(\nu) = \frac{\beta(h\nu - E_{opt})^n}{h\nu} \qquad (2)$$

In this equation, β is the bonding parameter and hν is the phonon energy. Figure-5 denotes the touch's plots of $(\alpha h\nu)^{1/2}$ and $(\alpha h\nu)^2$ with hν for Eu^{3+} doped glasses at 0.9 mol%.[10] The band gap of E_{opt} for direct and indirect transitions are 3.515 and 3.617 respectively. Table-3 displays the values of E_{opt} & ΔE (optical band gap and Urbach energy). The data show that as Eu^{3+} ions concentration grows, the optical band gap increases due to non-bridging oxygen ions causing localized energy states inside the band gap to alter the structural changes. The Urbach energy values in the table are inversely related to the optical band gap values. The reduction in Urbach energy as the concentration of Eu^{3+} ions increase indicates a lower number of defects in the glass system.

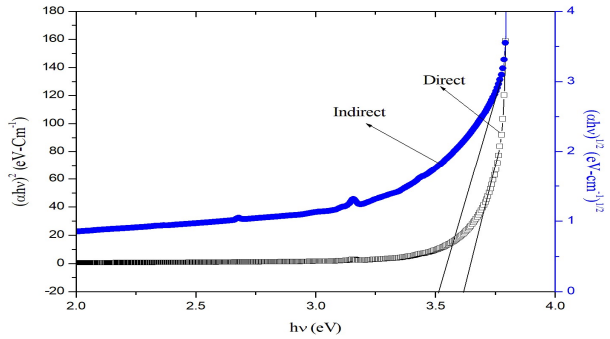

Fig.-5: Touch plots of $(\alpha h\nu)^2$ and $(\alpha h\nu)^{1/2}$ and hν for Eu 0.9 mol % of Eu^{3+} doped B_2O_3-ZnF_2-CaF_2-Al_2O_3 glasses

Nephelauxetic Ratio and Bonding Parameter

The nephelauxetic ratio with the bonding parameter is calculated to study the nature of Eu^{3+} ions. These values are computed using a formula:[11]

$$\beta = \frac{\nu_c}{\nu_a} \qquad (3)$$

The wave number in a given transition is represented by ν_c, while the wave number for the aqua-ions is represented by ν_a. The bonding parameter δ is denoted by:

$$\delta = \frac{1-\overline{\beta}}{\beta} \times 100 \qquad (4)$$

Table-4: Nephelauxetic Ratio ($\overline{\beta}$), Bonding Parameter (δ) Values Eu^{3+} Doped B_2O_3-ZnF_2- $CaF_2Al_2O_3$ Glasses

Transition	Observed band position (cm^{-1})	Aquo-ion (cm^{-1})	$\beta = \frac{\upsilon_c}{\upsilon_a}$				
			Eu 0.1	Eu 0.3	Eu 0.5	Eu 0.7	Eu 0.9
$^7F_0 \rightarrow {}^5L_6$	25445	25317	1.0076	1.0050	1.0050	1.0050	1.0050
$^7F_1 \rightarrow {}^5L_6$	25062	25000	1.0024	1.0024	1.0024	1.0024	1.0024
$^7F_1 \rightarrow {}^5D_3$	24271	24038	0.0121	1.0121	1.0048	1.0048	1.0121
$^7F_0 \rightarrow {}^5D_2$	21598	21519	1.0036	1.0036	1.0014	1.0014	1.0036
$^7F_0 \rightarrow {}^5D_1$	18832	19028	1.0009	1.0009	1.0009	1.0009	1.0009
$^7F_0 \rightarrow {}^7F_6$	4773	4980	0.9560	0.9570	0.9566	0.9588	0.9578
$^7F_1 \rightarrow {}^7F_6$	4531	4630	0.9816	0.9812	0.9812	0.9816	0.9812
	Glass Sample			$\overline{\beta}$		Δ	
	Eu 0.1			0.9948		0.5227	
	Eu 0.3			0.9946		0.5429	

	Eu 0.5		0.9931	0.6947
	Eu 0.7		0.9935	0.6542
	Eu 0.9		0.9947	0.5328

In the above table, the calculated average values of the nephelauxetic ratio $\overline{\beta}$ are shown. These parameters are entirely determined by the positive and negative values of the boding parameter (δ) respectively. The calculated values of β and δ are mentioned in Table-4. The covalent character of the Eu^{3+} ions is represented by a positive value of δ.

Oscillator Strength

The experimental values of the oscillator strength (f_{exp}) of the absorption bands are computed using the formula utilizing the absorption spectrum and the area under the absorption peak.

Where ε(ν) denotes the molar coefficient at frequency ν cm^{-1}. The equation for oscillator strength can be given as:[12]

$$f_{\exp} = 4.319 \times 19^{-9} \int \varepsilon(\nu) d\nu \qquad (5)$$

$$f_{cal} = \frac{8\pi^2 mc\nu}{3h(2J+1)} \left[\frac{(n^2+2)^2}{9n} \right] \sum_{\lambda=2,4,6} \Omega_\lambda (\varphi J \| U^\lambda \| \varphi' J')^2 \qquad (6)$$

Table-5: Experimental and Calculated Oscillator Strength of Eu^{3+} Doped B_2O_3-ZnF_2- CaF_2-Al_2O_3 Glasses

Transitions	Wavelength (nm)	Eu^{3+}	
		f_{exp} ($x10^{-6}$)	f_{cal} ($x10^{-6}$)
$^7F_0 \rightarrow {}^5L_6$	393	0.962	0.923
$^7F_0 \rightarrow {}^5D_2$	463	0.748	0.568
$^7F_0 \rightarrow {}^5D_1$	531	0.527	0.489
$^7F_0 \rightarrow {}^7F_6$	2095	2.293	1.634
$^7F_1 \rightarrow {}^7F_6$	2207	1.538	1.432
RMS	±0.3101		

Here m. c, h, v, and n are considered the stranded values, (2J+1) is the ground state degeneracy, $(n^2+2^2)/9n$ is the Lorentz correction, and Ω_λ =2, 4, 6is the unit tensor operator, the quality fitting parameters is determined by the formula:

$$\delta_{rms} = \left[\frac{(f_{\exp} - f_{cal})^2}{N} \right]^{1/2} \qquad (7)$$

The calculated values of f_{exp} and f_{cal} δ_{rms} are tabulated in Table-5.

Excitation Spectrum

The excitation spectrum of Eu^{3+} doped B_2O_3-ZnF_2-CaF_2-Al_2O_3 glasses is investigated in the wavelength range 350 - 600 nm. The intensity of peaks associated with electronic transitions from $^7F_0$ ground state to various excited states is observed in these spectra which are assigned to the transitions from 360 ($^5D_4$), 378 ($^5L_7$), 392 ($^5L_6$), 412 ($^5D_3$), 462 ($^5D_2$) and 530 ($^5D_1$) nm respectively.[13] Of these transitions, $^7F_0 \rightarrow {}^5L_6$ (392 nm) is the most noticeable and strong peak when compared to the others depicted in Fig.-6.

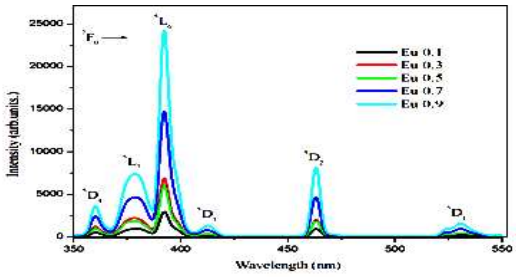

Fig.-6: Excitation spectra of Eu^{3+} doped B_2O_3-ZnF_2-CaF_2-Al_2O_3 glasses

Emission Spectrum

The emission spectrum of Eu^{3+}doped B_2O_3-ZnF_2-CaF_2-Al_2O_3 glasses is investigated using wavelengths ranging from 550 to 750 nm and a wavelength of excitation 392 nm. It has five emission transitions in the visible spectral region, such as $^5D_O \rightarrow {}^7F_J$ (J=0, 1, 2, 3, 4, 5) at 577, 589, 612, 650, and 699 nm. These distinctive peaks correspond to the 4f-4f transitions seen in Fig.-7. The graph shows that the intensity of these emissions increases as the Eu^{3+} ion level increases.[14] The strongest emission band is found at 612 nm and is composed of hypersensitive transitions determined using the ΔJ=±1selection rule. Figure-8 depicts an energy level diagram with many transitions. According to Fig.-7, Eu^{3+} ions in the ground state $^7F_0$ are excited to the energy state $^5L_6$, which is displayed in absorption. So due to the non-radiative transitions, the excitation of Eu^{3+} ions is changed to the lowest $^5D_0$ level. All electrons remain present for a long period at the state of $^5D_0$, which is considered a meta-stable state, and then go to the ground state by several transitions of $^7F_0$, $^7F_1$, $^7F_2$, $^7F_3$ and $^7F_4$.[15] The red emission transition is considered to be the ground state $^7F_0$ transition. The ratio offered to orange for the transitions $^5D_0 \rightarrow {}^7F_2$ to $^5D_0 \rightarrow {}^7F_1$ confirms this. According to Table-6, the R/O ratio falls as the concentration of Eu^{3+} ions increase. Of all the values of Eu^{3+} doped glasses, Eu 0.1 glass has comparatively high intensity compared to the other glasses, indicating a more asymmetric environment and more covalent bonds of Eu-O bond, which also provides strong agreement with the results of the bonding parameter.

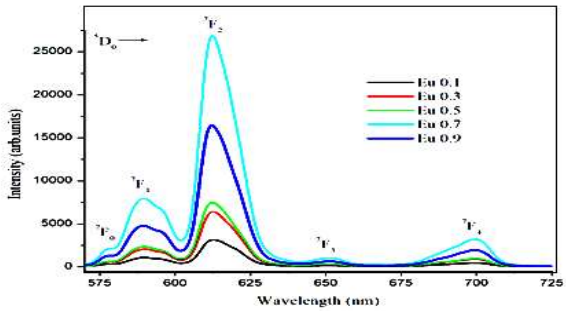

Fig.-7: Emission spectra of Eu^{3+} doped B_2O_3-ZnF_2-CaF_2-Al_2O_3 glasses

J-O Parameter

Due to some difficulties in the absorption spectrum, the J-O intensity parameter is estimated by emission spectra. Only a few transitions $^5D_1$, $^5D_2$, and $^5L_6$ are found with good intensity in the optical absorption spectra from $^7F_0$ and $^7F_1$. As a result, it is regarded as another method for determining the J-O parameter from emission spectra and transitions of the majority of the surrounding substance elements begin at zero (i.e., $^5D_0$), i.e., $^5D_0 \rightarrow {}^7F_J$ (J = 0, 1, 2, 3, 4). Nevertheless, the $^5D_0 \rightarrow {}^7F_6$ transition is not seen in the luminescence spectra because it is assumed to be zero.[16] Table-6 shows the J-O parameters derivative using this approach. In the majority of situations, the J-O parameters follow the pattern of $\Omega_2 > \Omega_4 > \Omega_6$. Around these three parameters, Ω_2 is connected to the local ions surrounding the RE ion site and has a substantial influence on covalency between ligands and RE^{3+} ions. Ω_4 and Ω_6 on the other hand are connected to the viscosity of the host glass matrix. Of the three parameters, Ω_2 is very strong, with the highest covalency and the lowest symmetry.

$$A_R = \frac{64\pi^4 \lambda_0^{\ 3}}{3h(2J+1)}\left[\frac{n(n^2+2)^2}{9} S_{ed} + n^2 S_{md}\right] \qquad (8)$$

Table-6: JO Intensity Parameters of Eu^{3+} Doped B_2O_3-ZnF_2-CaF_2-Al_2O_3 Glasses

Glass Samples	Ω_2x10^{-20} (cm^{-2})	Ω_4 x10^{-20} (cm^{-2})	Ω_6 x10^{-20} (cm^{-2})	Red to orange ratio ($^5D_o \rightarrow {}^7F_2$)/($^5D_o \rightarrow {}^7F_1$)
Eu 0.1	1.864	0.764	-	1.0397
Eu 0.3	1.752	0.635	-	1.0387
Eu 0.5	1.928	0.829	-	1.0387
Eu 0.7	2.169	1.325	-	1.0381
Eu 0.9	2.085	1.487	-	1.0387

Radiative Properties

The radiative characteristics were derived using J-O intensity parameters, and they are employed to expect the lasing capability for electric transitions dipole from excited to ground states. The radiative transitions probability A_R is given from initial to final state aJ → aJ' represented as

The total radiative property is expressed as the number of radiative transition probabilities from the initial state to the stimulated state given by:[17]

$$A_\tau = \sum A \tag{9}$$

The radiative lifetime (τ_R) can be measured using the formula:

$$\tau_R = \frac{1}{A_\tau} \tag{10}$$

According to the below formula, the optical potentiality of prepared glasses is calculated by using the branching ratio (βr),

$$\beta_\gamma = \frac{A}{A\tau} \tag{11}$$

Table-7 displays doped the radiative characteristics of B_2O_3-ZnF_2-CaF_2-Al_2O_3 glasses, including A_R and Aτ (transition probability and total transition probability). The table shows that the transitions probability (A_R) and total radiative probability (Aτ) rise as the concentrations of Eu^{3+} ions increase. $^5D_0 \rightarrow {}^7F_2$ has the highest transition probability of other transitions.

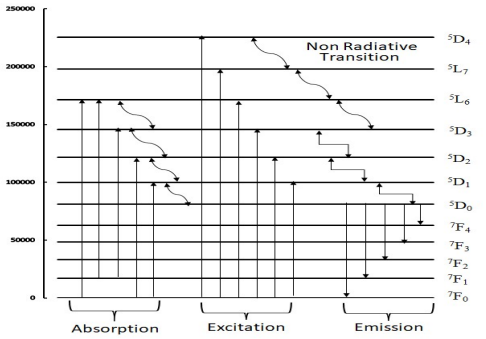

Fig.-8: Partial Energy level diagram of Eu^{3+} doped B_2O_3-ZnF_2-CaF_2-Al_2O_3 glasses

Table-7: Radiative Transition Probability (A), Total Transition Probability (A_T), Branching Ratio (β_R) and Radiative Life Time (τ_{rad}) of Eu^{3+} Doped B_2O_3-ZnF_2-$CaF_2Al_2O_3$ Glasses

Transition from $^5D_0 \rightarrow$	Eu 0.1		Eu 0.3		Eu 0.5		Eu 0.7		Eu 0.9	
	A_{rad}	β_r	A_{rad}	β_r	A_{rad}	β_r	A_{rad}	β_r	A_{rad}	β_r
$^7F_1$	76.82	35.28	78.94	34.84	81.25	34.75	83.79	34.28	85.27	33.25
$^7F_2$	82.65	37.96	86.27	38.07	89.36	38.22	91.34	37.37	98.54	38.42
$^7F_4$	58.24	26.75	61.34	27.07	63.14	27.01	68.23	27.92	72.63	28.32
A_τ	217.71		226.55		233.75		244.36		256.44	
τ_r	0.0045		0.0044		0.0042		0.0040		0.0038	

Table-8: The Color Coordinate (x, y) of CIE 1931 Chromaticity and Correlated Color Temperature (CCT, K) of Eu^{3+} doped B_2O_3-ZnF_2-$CaF_2Al_2O_3$ glasses

Glass Samples	CIE color coordinates		CCT (K)
	x	Y	
Eu 0.1	0576	0.418	1389
Eu 0.3	0.598	0.407	1197
Eu 0.5	0.619	0.394	1066
Eu 0.7	0.625	0.386	1034
Eu 0.9	0.628	0.378	1021

Evaluation of Color Coordinates

Figure-9 depicts the CIE colour coordinates (Commission International d'eclairage) for Eu^{3+} doped B_2O_3-ZnF_2-CaF_2-Al_2O_3 glasses. They are used to analyze emission intensities in order to determine the dominant emission wavelength by employing emission spectra with excitation wavelengths of 392 nm. The computed (x, y) values with range of 0.576-0.628 and 0.418-0.378, which is close to typical red color values (0.67, 0.33), indicating that the analyzed glasses are in the orange-red light field.[18] The corrected color temperature was calculated to find out the quality of light by using the formula,

$$CCT = - 449n^3 + 3525n^2 - 6823n + 5520.3 \quad (12)$$

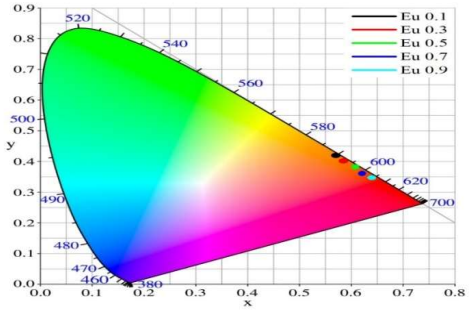

Fig.-9: The chromaticity diagram of Eu^{3+} doped B_2O_3-ZnF_2-CaF_2-Al_2O_3 glasses

Consider the inverse slope of the line (x_e = 0.332 and y_e=0.186) with n = x-x_e / y-y_e. Table-8 displays the computed values as well as the x and y coordinators. These results also showed that the examined glasses are the potential candidates for the red-light emitting source.

CONCLUSION

Using a conventional melt quenching technique, different concentrations of Eu^{3+} doped B_2O_3-ZnF_2-CaF_2-Al_2O_3 glasses were prepared, and the materials were characterized for various applications using spectroscopic techniques such as optical absorption, excitation, emission, as well as physical properties, XRD, and FTIR techniques. Based on all of the physical properties, it can be deduced that as the concentrations of Eu^{3+} ions increase, the compactness of the glass materials also increases. The FTIR spectra show a B-O-B linkage as well as a borate network with BO_3 and BO_4 structural units and AlO_4 structural units. The optical absorption spectra show that $^7F_0 \rightarrow {}^5F_6$ (393 nm) is the most intense band. The nephelauxetic ratio demonstrates that the examined glasses are covalent in nature. The emission spectra show five intensity bands at 577, 589, 612, 650, and 699 nm, which correspond to $^5D_0$, $^7F_0$, $^7F_1$, $^7F_2$, $^7F_3$, and $^7F_4$ transitions, respectively. The J-O values are derived from the luminescence intensity ratio of $^5D_0 \rightarrow {}^7F_J$ (J=2, 4). Of the numerous emission transitions, $^5D_0 \rightarrow {}^7F_2$ has maximum (Ω_2) intensity and is appropriate for strong red emission. The CIF (XY) coordinates are in the red-light zone, and the CCT values show that the examined glasses are acceptable for red-light LEDs.

ACKNOWLEDGEMENTS

Authors acknowledge the cooperation and support of the authorities of their institutions.

CONFLICT OF INTERESTS

The authors declare that there is no conflict of interest.

AUTHOR CONTRIBUTIONS

All the authors contributed significantly to this manuscript, participated in reviewing/editing, and approved the final draft for publication. The research profile of the authors can be verified from their ORCID IDs, given below:

N Rajyalakshmi http://orchid.org/0000-0002-6513-147X
Santhan Kumar Jalli http://orchid.org/0000-0001-8188-1ss45X
K Venkatarao http://orchid.org/0000-0001-7091-2986
Sandhya Cole http://orchid.org/0000-0002-1827-2149

REFERENCES

1. K. Honga, M. Kima, M. GyuHaa, J.Pil Kim, *Journal of Non-Crystalline Solids,* **505**, 400(2019), https://doi.org/10.1016/j.jnoncrysol.2018.10.0s30
2. A.A. Andrade, M.F. Coutinho, M.P.P. de Castro, H. Vargas, *Journal of Non-Crystalline Solids,* **352**, 3624(2006), https://doi:10.1016/j.jnoncrysol.2006.03.092
3. S.A. Lourenc-o, N.O. Dantas, E.O. Serqueira, W.E.F. Ayta, A.A. Andrade, *Journal of Luminescence,* **131**, 850(2011), https://doi:10.1016/j.jlumin.2010.11.028
4. N. Vijaya, C.K. Jayasankar, *Journal of Molecular Structure,* **1036**, 42(2012), https://doi.org/10.1016/j.molstruc.2012.09.037
5. F. Jiang, S. Sha, S. Li, S. Xu, H. Xu, X. Mei, Y. Zhang, *Ceramics International*, **47**, 13776(2021), https://doi.org/10.1016/j.ceramint.2021.01.241
6. B.Tirumala Rao1 and Sandhya Cole, *Rasayan Journal of Chemistry,* **12(3)**, 1557(2019), http://dx.doi.org/10.31788/RJC.2019.1235089
7. K. Mariselvam, R. Arun Kumar, *Optik - International Journal for Light and Electron* Optics, **226**, 165910(2021), https://doi.org/10.1016/j.ijleo.2020.165910
8. P. Ramesh, Vinod Hegde, K. Keshavamurthy, A.G. Pramod, G. Jagannath, *Optical Materials,* **116**, 111102(2021), https://doi.org/10.1016/j.optmat.2021.111102
9. L. Yuliantini, M. Djamal, R. Hidayat, P. Yasaka, J. Kaewkhao, K. Boonin, *Materials Today: Proceedings,* **17**, 1815(2019), https://doi.org/10.1016/j.matpr.2019.06.218
10. N. Kawano, K. Shinozaki, D. Nakauchi, H. Kimura, M.Akatsuka, T.Yanagida, *Radiation Physics and Chemistry*, **190**, 109785(2022), https://doi.org/10.1016/j.radphyschem.2021.109785
11. R.N.A. Prasad, B. Venkata Siva, K. Neeraja, N. Krishna Mohan, J. I. Rojas, *Journal of Luminescence,* **230**, 117666(2021), https://doi.org/10.1016/j.jlumin.2020.117666
12. K. Pavani, J. Suresh Kumar, T. Chengaiah, L. Rama Moorthy, *Journal of Molecular Structure,* **1028**, 170(2012), http://dx.doi.org/10.1016/j.molstruc.2012.06.037
13. P. Meejitpaisan, C. Kedkaew, J. Kaewkha, *Materials Today: Proceedings*, **5**, 13926(2018). https://doi.org/10.1016/j.matpr.2018.02.042
14. Tayaramma D.P.V. Jalluri, K.V. Sriram, B. Rudraswamy, Vinod Hegde, *Infrared Physics & Technology,* **116**, 103784(2021), https://doi.org/10.1016/j.infrared.2021.103784
15. MelisGokce, Journal *of Non-Crystalline Solids,* **505**, 272(2019), https://doi.org/10.1016/j.jnoncrysol.2018.11.011
16. N. Wantana, E. Laewnuam, B. Damdee, S. Kaewjaeng, S. Kothan, *Journal of Luminescence,* **194**, 75-81(2018), https://doi.org/10.1016/j.jlumin.2017.10.004
17. N. Kiran, *Journal of Molecular Structure*, **1065-1066**, 93-98 (2014), https://doi.org/10.1016/j.molstruc.2014.02.047
18. P.P. Pawar, S.R. Munishwar, R.S. Gedam, *Journal of Luminescence*, **181**, 367(2017), https://doi.org/10.1016/j.jlumin.2018.04.026

[RJC- 8425/2023]